Tunable phononic crystals with anisotropic inclusions

Sz-Chin Steven Lin and Tony Jun Huang*

Department of Engineering Science and Mechanics, The Pennsylvania State University, University Park, Pennsylvania 16802, USA

(Received 13 January 2011; revised manuscript received 21 March 2011; published 18 May 2011)

We present a theoretical study on the tunability of phononic band gaps in two-dimensional phononic crystals consisting of various anisotropic cylinders in an isotropic host. A two-dimensional plane-wave expansion method was used to analyze the band diagrams of the phononic crystals; the anisotropic materials used in this work include cubic, hexagonal, trigonal, and tetragonal crystal systems. By reorienting the anisotropic cylinders, we show that phononic band gaps for bulk acoustic waves propagating in the phononic crystal can be opened, modulated, and closed. The methodology presented here enables enhanced control over acoustic metamaterials which have applications in ultrasonic imaging, acoustic therapy, and nondestructive evaluation.

DOI: 10.1103/PhysRevB.83.174303 PACS number(s): 63.20.−e, 43.20.+g, 46.40.Cd

I. INTRODUCTION

Understanding the propagation behavior of acoustic waves in periodic composite structures is important for many acoustic-based applications. These periodic composite structures, known as phononic crystals, are composed of arrays of elastic inclusions embedded in a host material with different elastic properties.[1] For wavelengths on the scale of the structure's periodicity, phononic crystals exhibit complete phononic band gaps: frequency ranges where the vibration of acoustic waves is suppressed in any mode.[2–4] Phononic band gaps result from the destructive interference between incident acoustic waves and reflections from these periodic scatterers; as such, they have been employed to obtain perfect acoustic mirrors,[5] filters,[6] switches,[7,8] and lenses[9–11] at designated frequencies. In addition, vibrations at frequencies in the band gap can be strongly localized to defects in the phononic crystal, making them practical for acoustic resonators[12,13] and waveguides.[14–16]

At frequencies outside the phononic band gap, the band diagrams for phononic crystals are distorted when compared to a homogeneous, isotropic material. Isotropic media have circular equal-frequency contours (EFCs), whereas the EFCs in a phononic crystal can be highly anisotropic, especially at frequencies near the phononic band gaps. In general, the propagation direction of an acoustic wave beam is normal to the EFCs of the medium per the relation $v_g = \nabla_k \omega(k)$, where v_g is the group velocity, ω is the angular velocity, and k is the wave vector. As a result, large bending effects such as negative refraction,[17–22] self-collimation,[23] and acoustic mirages[24] can be obtained within phononic crystals due to the anisotropic EFCs. Phononic crystals are identified as acoustic metamaterials because of this extraordinary behavior, and their applications have been extended from bulk acoustic waves[25–27] to surface acoustic waves,[28,29] and more recently to plate waves.[30–32]

Much of the existing research on phononic crystals focuses on understanding how the width and position of phononic band gaps depend upon the constitutive parameters (e.g., geometry, composition, and material properties) of the structures.[33] This focus is mainly due to the fact that almost all phenomena exhibited by phononic crystals rely on the formation of a phononic band gap. Explicit control of a phononic band gaps yields desirable operation parameters and improves overall performance for phononic crystal-based applications. Recent studies have shown that phononic band gaps can be tuned by (i) physical rotation[34–36] or relocation[37] of inclusions to modify the dispersion relation for acoustic waves, (ii) mechanical deformation of the structure by an external stress,[38] (iii) actively changing the elastic properties of the constitutive materials through application of a strong external stimulus (e.g., electric and magnetic fields),[8,39,40] and (iv) changing the acoustic velocities in ferroelectric materials through a temperature variation induced phase transition.[41,42] For cases (i) and (ii), isotropic materials are usually chosen to form the heterogeneous structures where a change in geometry accounts for the tunability of the phononic band gaps. On the contrary, a number of anisotropic materials have been utilized to build tunable phononic crystals with approaches (iii) and (iv), as they are more sensitive to perturbations in the environment. Because of this sensitivity, the rotation and/or relocation of anisotropic inclusions in a phononic crystal could potentially have greater flexibility and stronger effects in tuning phononic band gaps, however, no comprehensive research has been done yet.

In this work, we present a comprehensive study on the tunability of phononic band gaps in two-dimensional phononic crystals consisting of anisotropic cylinders in an isotropic host. We demonstrate that control of the phononic band gaps results from the reorientation of the anisotropic cylinders. The anisotropic materials considered in this study include cubic, hexagonal, trigonal, and tetragonal materials. A two-dimensional plane-wave expansion (PWE) method[28] is used to calculate the variation in the phononic band gaps upon the reorientation of the anisotropic cylinders. Our results show that the band gaps of a phononic crystal can be broadly tuned by the proposed method, allowing enhanced control over acoustic metamaterials.

In Sec. II, we introduce the model and method used to calculate the band gaps of the phononic crystals. In Sec. III, we present and discuss the tunability of two-dimensional phononic crystals with cubic, hexagonal, trigonal, and tetragonal cylinders, respectively. Finally, we present a summary in Sec. IV.

II. FORMULATION

Figure 1 gives a schematic which illustrates the geometry of the periodic composite structures used in our work. The

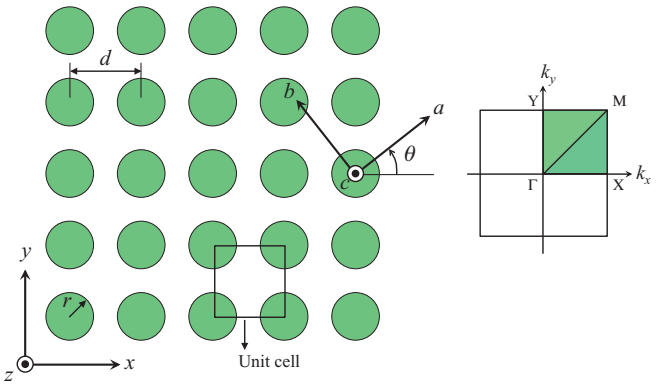

FIG. 1. (Color online) The left diagram shows the top view of an infinite two-dimensional square-lattice phononic crystal. The right diagram shows the corresponding first Brillouin zone of the unit cell.

anisotropic cylinders with radius r are arranged in a two-dimensional square array with lattice spacing d and embedded in a homogeneous host material. A global Cartesian coordinate system xyz is set with the z axis parallel to the cylinder axis and x and y axes along the lattice axes of the square array. In the absence of a body force and temperature factor,[42,43] the equation of motion for the displacement vector in a periodic composite structure can be written as

$$\rho(\mathbf{r})\ddot{u}_i(\mathbf{r},t) = \partial_j[c_{ijmn}(\mathbf{r})\partial_n u_m(\mathbf{r},t)], \tag{1}$$

where $\mathbf{r} = (\mathbf{x},z) = (x,y,z)$ is the position vector with respect to the global coordinate system xyz, t is the time variable, and $\rho(\mathbf{r})$ and $c_{ijmn}(\mathbf{r})$ are the position-dependent mass density and elastic stiffness tensor, respectively. In this section, the constitutive materials (cylinders and host) of the periodic composite structure are of the lowest symmetry, i.e., belonging to the triclinic symmetry.

The wave behavior in this two-dimensional phononic crystal is very complicated and highly sensitive to the frequency and direction of the propagating wave due to the periodicity of the structure and the anisotropy of the constitutive materials. The wave equation, Eq. (1), can be solved by a number of numerical methods, such as PWE methods,[28] multiple-scattering theory (MST),[44–46] and finite-difference time-domain (FDTD) methods.[14] In this work we use a two-dimensional PWE method to solve for the dispersion relations of the acoustic waves because of its strength in analyzing structures containing anisotropic materials.[28] When only bulk acoustic modes are considered, the PWE method dictates that the equation of motion for a two-dimensional periodic composite structure can be expanded into a Fourier series with respect to reciprocal-lattice vectors G and G', and rewritten as an eigenvalue problem:

$$\begin{bmatrix} \omega^2\rho_{\mathbf{G}-\mathbf{G}'} + M^1_{\mathbf{G}-\mathbf{G}'} & L^1_{\mathbf{G}-\mathbf{G}'} & U^1_{\mathbf{G}-\mathbf{G}'} \\ L^2_{\mathbf{G}-\mathbf{G}'} & \omega^2\rho_{\mathbf{G}-\mathbf{G}'} + M^2_{\mathbf{G}-\mathbf{G}'} & U^2_{\mathbf{G}-\mathbf{G}'} \\ W^1_{\mathbf{G}-\mathbf{G}'} & W^2_{\mathbf{G}-\mathbf{G}'} & \omega^2\rho_{\mathbf{G}-\mathbf{G}'} + M^3_{\mathbf{G}-\mathbf{G}'} \end{bmatrix} \cdot \begin{bmatrix} A^1_{\mathbf{G}'} \\ A^2_{\mathbf{G}'} \\ A^3_{\mathbf{G}'} \end{bmatrix} \equiv \mathbf{MU} = 0, \tag{2}$$

where $\mathbf{U}$ is the eigenvector and $\mathbf{M}$ is a function of the Block wave vector $\mathbf{k}$, angular frequency ω, Fourier coefficients of mass density $\rho_{\mathbf{G}-\mathbf{G}'}$ and components of elastic stiffness tensor $c^{ij}_{\mathbf{G}-\mathbf{G}'}$. The expressions of the nine matrix entries in Eq. (2) are

$$\begin{aligned} M^1_{\mathbf{G}-\mathbf{G}'} &= \left[b_1 c^{11}_{\mathbf{G}-\mathbf{G}'} + b_2 c^{16}_{\mathbf{G}-\mathbf{G}'} + b_3 c^{61}_{\mathbf{G}-\mathbf{G}'} + b_4 c^{66}_{\mathbf{G}-\mathbf{G}'}\right], \\ M^2_{\mathbf{G}-\mathbf{G}'} &= \left[b_1 c^{66}_{\mathbf{G}-\mathbf{G}'} + b_2 c^{62}_{\mathbf{G}-\mathbf{G}'} + b_3 c^{26}_{\mathbf{G}-\mathbf{G}'} + b_4 c^{22}_{\mathbf{G}-\mathbf{G}'}\right], \\ M^3_{\mathbf{G}-\mathbf{G}'} &= \left[b_1 c^{55}_{\mathbf{G}-\mathbf{G}'} + b_2 c^{54}_{\mathbf{G}-\mathbf{G}'} + b_3 c^{45}_{\mathbf{G}-\mathbf{G}'} + b_4 c^{44}_{\mathbf{G}-\mathbf{G}'}\right], \end{aligned} \tag{3}$$

$$\begin{aligned} L^1_{\mathbf{G}-\mathbf{G}'} &= \left[b_1 c^{16}_{\mathbf{G}-\mathbf{G}'} + b_2 c^{12}_{\mathbf{G}-\mathbf{G}'} + b_3 c^{66}_{\mathbf{G}-\mathbf{G}'} + b_4 c^{62}_{\mathbf{G}-\mathbf{G}'}\right], \\ L^2_{\mathbf{G}-\mathbf{G}'} &= \left[b_1 c^{16}_{\mathbf{G}-\mathbf{G}'} + b_2 c^{66}_{\mathbf{G}-\mathbf{G}'} + b_3 c^{21}_{\mathbf{G}-\mathbf{G}'} + b_4 c^{26}_{\mathbf{G}-\mathbf{G}'}\right], \end{aligned} \tag{4}$$

$$\begin{aligned} U^1_{\mathbf{G}-\mathbf{G}'} &= \left[b_1 c^{15}_{\mathbf{G}-\mathbf{G}'} + b_2 c^{14}_{\mathbf{G}-\mathbf{G}'} + b_3 c^{65}_{\mathbf{G}-\mathbf{G}'} + b_4 c^{64}_{\mathbf{G}-\mathbf{G}'}\right], \\ U^2_{\mathbf{G}-\mathbf{G}'} &= \left[b_1 c^{65}_{\mathbf{G}-\mathbf{G}'} + b_2 c^{64}_{\mathbf{G}-\mathbf{G}'} + b_3 c^{25}_{\mathbf{G}-\mathbf{G}'} + b_4 c^{24}_{\mathbf{G}-\mathbf{G}'}\right], \end{aligned} \tag{5}$$

$$\begin{aligned} W^1_{\mathbf{G}-\mathbf{G}'} &= \left[b_1 c^{51}_{\mathbf{G}-\mathbf{G}'} + b_2 c^{56}_{\mathbf{G}-\mathbf{G}'} + b_3 c^{41}_{\mathbf{G}-\mathbf{G}'} + b_4 c^{46}_{\mathbf{G}-\mathbf{G}'}\right], \\ W^2_{\mathbf{G}-\mathbf{G}'} &= \left[b_1 c^{56}_{\mathbf{G}-\mathbf{G}'} + b_2 c^{52}_{\mathbf{G}-\mathbf{G}'} + b_3 c^{46}_{\mathbf{G}-\mathbf{G}'} + b_4 c^{42}_{\mathbf{G}-\mathbf{G}'}\right], \end{aligned} \tag{6}$$

where

$$\begin{aligned} b_1 &= -(G_1 + k_1)(G'_1 + k_1), \\ b_2 &= -(G_1 + k_1)(G'_2 + k_2), \\ b_3 &= -(G_2 + k_2)(G'_1 + k_1), \\ b_4 &= -(G_2 + k_2)(G'_2 + k_2). \end{aligned} \tag{7}$$

In the above equations, Voigt's notation has been used to express the Fourier coefficients of the elastic stiffness tensor $c^{ij}_{\mathbf{G}-\mathbf{G}'}$. The eigenfrequencies of the bulk acoustic modes can be obtained by setting

$$\det(\mathbf{M}) = 0. \tag{8}$$

Once the eigenfrequencies are obtained, the relative amplitude of the displacement for each eigenmode can be solved by substituting the eigenfrequencies into Eq. (2).

As the anisotropic cylinders are rotated through an angle θ about the cylinder axis (z axis), the crystalline axes of the cylinders are reoriented accordingly. The rotation of the cylinders changes the value of the Fourier coefficients in the elastic stiffness tensor $c^{ij}_{\mathbf{G}-\mathbf{G}'}$ in Eqs. (3)–(6), which influences the acoustic wave propagation behavior in the periodic composite structure. We define another Cartesian coordinate system abc with the c axis parallel to the z axis of the global system, as shown in Fig. 1, to track the orientation of the anisotropic cylinders.

The transformation of the coordinate position vector between the global and cylinder coordinate systems can be achieved by

$$\begin{bmatrix} a \\ b \\ c \end{bmatrix} = \begin{bmatrix} \cos\theta & \sin\theta & 0 \\ -\sin\theta & \cos\theta & 0 \\ 0 & 0 & 1 \end{bmatrix} \cdot \begin{bmatrix} x \\ y \\ z \end{bmatrix}. \tag{9}$$

Consequently, the elastic stiffness tensor of the rotated cylinders in terms of the global coordinate system xyz can be obtained by transforming the rotational coordinate:[47]

$$\mathbf{c}' = \mathbf{T}\mathbf{c}\mathbf{T}^t, \tag{10}$$

where

$$\mathbf{T} = \begin{bmatrix} \cos^2\theta & \sin^2\theta & 0 & 0 & 0 & \sin 2\theta \\ \sin^2\theta & \cos^2\theta & 0 & 0 & 0 & -\sin 2\theta \\ 0 & 0 & 1 & 0 & 0 & 0 \\ 0 & 0 & 0 & \cos\theta & -\sin\theta & 0 \\ 0 & 0 & 0 & \sin\theta & \cos\theta & 0 \\ -\sin\theta\cos\theta & \sin\theta\cos\theta & 0 & 0 & 0 & \cos 2\theta \end{bmatrix} \tag{11}$$

is the transformation matrix and $\mathbf{T}^t$ is the transpose of $\mathbf{T}$. Once the elastic stiffness tensor $\mathbf{c}'$ is obtained, the new dispersion relations for the bulk acoustic modes can be calculated by substituting $\mathbf{c}\prime$ back into Eqs. (3)−(6) and solving the eigenvalue problem.

The elastic material properties used in our work are listed in Table I.[47] The elastic stiffness components given in Table I refer to the global coordinate axes x, y, z that coincide with the crystalline axes X, Y, Z, i.e., acoustic waves propagate in the XY plane of the anisotropic materials. When acoustic waves do not propagate in the XY plane of the cylinders, i.e., the cylinder coordinate axes a, b, c do not coincide with the crystalline axes X, Y, Z, corresponding coordinate transformations must be applied to the elastic stiffness tensor of the cylinders before solving the eigenvalue problem. As acoustic waves propagate in the XZ plane of the cylinders, for example, the embedded crystal experiences a clockwise rotation through 90° about the crystalline X axis. Or when acoustic waves propagate in a meridian plane, the crystal rotates through 45° about the crystalline Z axis followed by 90° about the crystalline X axis. The coordinate transformation matrices for a rotation through an angle ξ about the crystalline X axis and an angle η about the crystalline Y axis are

$$\mathbf{T}_X = \begin{bmatrix} 1 & 0 & 0 & 0 & 0 & 0 \\ 0 & \cos^2\xi & \sin^2\xi & \sin 2\xi & 0 & 0 \\ 0 & \sin^2\xi & \cos^2\xi & -\sin 2\xi & 0 & 0 \\ 0 & -\sin\xi\cos\xi & \sin\xi\cos\xi & \cos 2\xi & 0 & 0 \\ 0 & 0 & 0 & 0 & \cos\xi & -\sin\xi \\ 0 & 0 & 0 & 0 & \sin\xi & \cos\xi \end{bmatrix} \tag{12}$$

and

$$\mathbf{T}_Y = \begin{bmatrix} \cos^2\eta & 0 & \sin^2\eta & 0 & -\sin 2\eta & 0 \\ 0 & 1 & 0 & 0 & 0 & 0 \\ \sin^2\eta & 0 & \cos^2\eta & 0 & \sin 2\eta & 0 \\ 0 & 0 & 0 & \cos\eta & 0 & \sin\eta \\ \sin\eta\cos\eta & 0 & -\sin\eta\cos\eta & 0 & \cos 2\eta & 0 \\ 0 & 0 & 0 & -\sin\eta & 0 & \cos\eta \end{bmatrix}, \tag{13}$$

respectively. The coordinate transformation matrix for a rotation about the crystalline Z axis is the same as the one defined in Eq. (11).

TABLE I. Elastic properties of the materials used in this paper (Ref. 47).

Material	Symmetry	Density(kg/m^3)	Elastic stiffness ($\times 10^{10}$ N/m^2)						
			C_{11}	C_{12}	C_{13}	C_{14}	C_{33}	C_{44}	C_{66}
Epoxy	isotropic	1180	0.761					0.159	
GaAs	cubic	5307	11.88	5.38				5.94	
ZnO	hexagonal	5680	20.97	12.11	10.51		21.09	4.247	
Quartz	trigonal	2651	8.674	0.699	1.191	1.791	10.72	5.794	
TiO_2	tetragonal	4260	26.6	17.33	13.62		46.99	12.39	18.86

III. NUMERICAL RESULTS

A. Cubic inclusions: GaAs/epoxy square lattice

Here we consider a two-dimensional phononic crystal consisting of a square array of circular gallium arsenide (GaAs) cylinders embedded in a homogeneous epoxy background. The phononic crystal has a lattice spacing d in both the x and y directions. Bulk acoustic waves propagate along the XY plane [(001) plane] in crystalline GaAs, thus no coordinate transformations need to be applied to the elastic stiffness tensor of the cylinders. GaAs belongs to the cubic crystal system while the epoxy is isotropic. The elastic stiffness tensor of a cubic material has the form

$$c = \begin{bmatrix} c_{11} & c_{12} & c_{12} & 0 & 0 & 0 \\ c_{12} & c_{11} & c_{12} & 0 & 0 & 0 \\ c_{12} & c_{12} & c_{11} & 0 & 0 & 0 \\ 0 & 0 & 0 & c_{44} & 0 & 0 \\ 0 & 0 & 0 & 0 & c_{44} & 0 \\ 0 & 0 & 0 & 0 & 0 & c_{44} \end{bmatrix}. \quad (14)$$

The slowness surfaces of bulk acoustic waves propagating in the XY plane of GaAs are shown in Fig. 2(a). It can be seen in this figure that the pure shear mode is isotropic, while the quasilongitudinal and quasishear modes are anisotropic with an eightfold symmetry. We expect that a cylinder rotation will change the band diagrams of the phononic crystal, including the width and position of the phononic band gaps.

Note that the elastic stiffness components $c_{14} = c_{41}$, $c_{15} = c_{51}$, $c_{24} = c_{42}$, $c_{25} = c_{52}$, $c_{46} = c_{64}$, and $c_{56} = c_{65}$ of cubic and isotropic materials are zero; as a result, the Fourier components in Eqs. (5) and (6) vanish ($U^1_{G-G'} = U^2_{G-G'} = W^1_{G-G'} = W^2_{G-G'} = 0$). The $\mathbf{M}$ matrix in Eq. (2) can therefore be decoupled into two different polarization modes of bulk acoustic waves as

$$\begin{bmatrix} \omega^2\rho_{\mathbf{G}-\mathbf{G}'} + M^1_{\mathbf{G}-\mathbf{G}'} & L^1_{\mathbf{G}-\mathbf{G}'} \\ L^2_{\mathbf{G}-\mathbf{G}'} & \omega^2\rho_{\mathbf{G}-\mathbf{G}'} + M^2_{\mathbf{G}-\mathbf{G}'} \end{bmatrix} \cdot \begin{bmatrix} A^1_{\mathbf{G}'} \\ A^2_{\mathbf{G}'} \end{bmatrix} = 0 \quad (15)$$

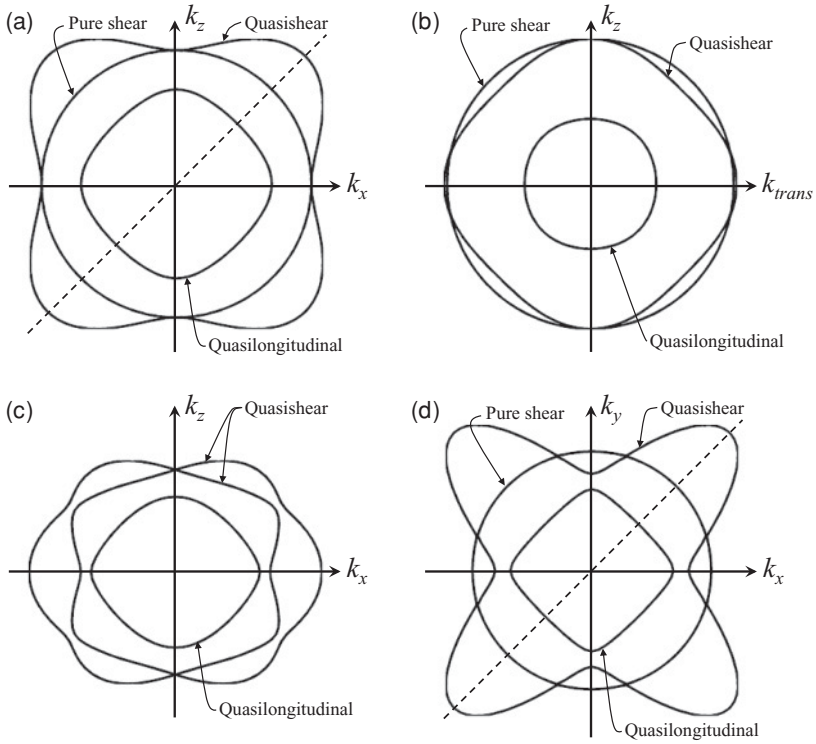

FIG. 2. Slowness surfaces of bulk acoustic waves propagating in (a) the XZ plane of GaAs, (b) the meridian plane of ZnO, (c) the XZ plane of quartz, and (d) the XY plane of TiO_2.

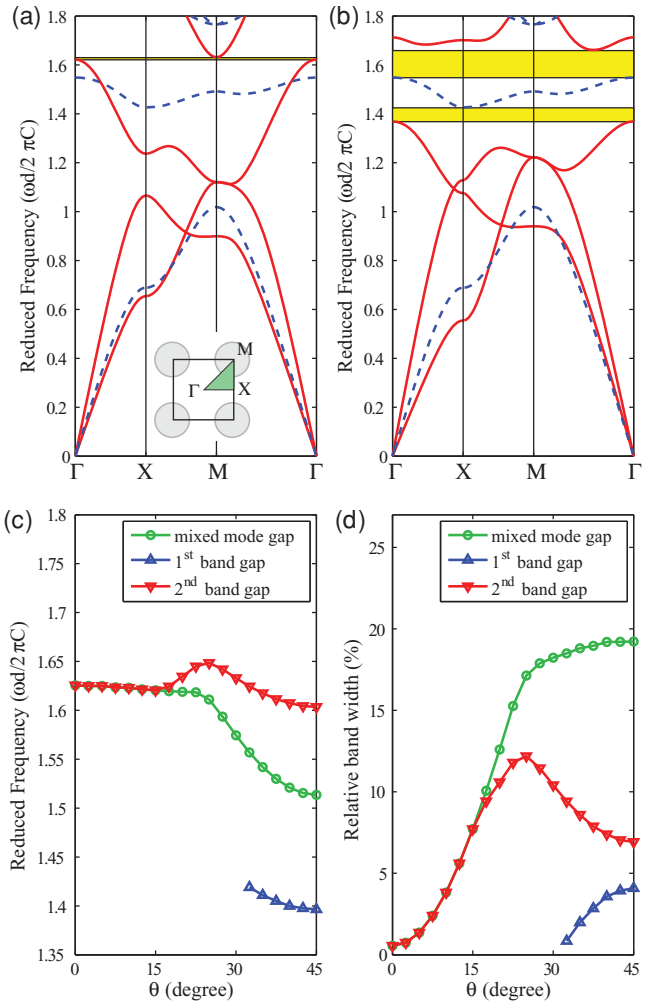

FIG. 3. (Color online) Dispersion relations for bulk modes of a GaAs (*XZ* plane)/epoxy square-lattice phononic crystal with a filling fraction of 0.65 and a cylinder rotation angle of (a) 0° and (b) 45°; (c) and (d) depict the angular dependence of the midgap frequency and relative bandwidth of the phononic band gaps, respectively.

for the mixed polarization modes [i.e., longitudinal (L) and shear horizontal (SH) modes with polarization in the xy plane] and

$$\left[\omega^2 \rho_{\mathbf{G}-\mathbf{G}'} + M^3_{\mathbf{G}-\mathbf{G}'}\right] \cdot \left[A^3_{\mathbf{G}'}\right] = 0 \tag{16}$$

for the transverse polarization mode [i.e., shear vertical (SV) mode with polarization along the z axis]. The mixed polarization modes correspond to the quasilongitudinal and quasishear modes in GaAs [Fig. 2(a)], and the transverse polarization mode corresponds to the pure shear mode.

Figure 3(a) shows the calculated dispersion relations for bulk acoustic waves propagating in a GaAs/epoxy phononic crystal with a filling fraction of $f = 0.65$ and a cylinder rotation angle of $\theta = 0$. The vertical axis of the dispersion relations gives the reduced frequency $\Omega = \omega d/2\pi C$ where C is the transverse wave velocity in epoxy, and the horizontal axis is the reduced wave vector $\mathbf{K} = kd/\pi$ along the periphery of the irreducible part (triangle ΓXM) in the first Brillouin zone. We used 121 reciprocal-lattice vectors in all calculations conducted in this paper to ensure the convergence of the PWE method. The red solid and blue dashed lines in Fig. 3(a) represent the mixed polarization and transverse polarization modes, respectively. The GaAs/epoxy phononic crystal demonstrates a narrow phononic band gap ranging from $\Omega = 1.621$ to $\Omega = 1.630$ with a relative bandwidth (phononic band-gap width divided by midgap frequency) of 0.55%. The yellow colored area in the figure indicates the location of the phononic band gap. When the GaAs cylinders are rotated through an angle of 45° about the cylinder axis, the elastic stiffness tensor changes with respect to the global coordinate system xyz; the corresponding dispersion relations are displayed in Fig. 3(b). Comparing Fig. 3(b) with Fig. 3(a), the shape of the mixed polarization modes (red solid lines) deforms greatly. However, the dispersion relation for the transverse polarization mode (blue dashed lines) is not altered at all after cylinder rotation because the Fourier components in $M^3_{\mathbf{G}-\mathbf{G}'}$ do not vary with the coordinate transformation. The 45°-cylinder-rotated GaAs/epoxy phononic crystal exhibits two phononic band gaps, separated by the second band of the vertical polarization mode, extending from $\Omega = 1.368$ to $\Omega = 1.425$ (relative bandwidth 4.1%) and from $\Omega = 1.548$ to $\Omega = 1.659$ (relative bandwidth 6.9%), respectively.

To further investigate the geometric dependence of the dispersion relations of the GaAs/epoxy phononic crystal, we calculated the midgap frequency and relative bandwidth of the phononic band gaps for cylinder rotation angles from 0° to 45° with an increment of 2.5°, as shown in Figs. 3(c) and 3(d), respectively. This angular range is sufficient because the angular dependence of the phononic band gaps is symmetric about $\theta = 45°$. We find that the first (lower frequency) phononic band gap only appears when $\theta > 30°$. The midgap frequency of this band gap decreases with θ while the gap width increases with θ. The second (higher frequency) phononic band gap exists throughout all rotation angles; it is located between the third and fourth frequency bands of the mixed polarization mode for $\theta \leqslant 15°$ and between the second frequency band of the transverse polarization mode and the fourth frequency band of the mixed polarization mode for $15° < \theta \leqslant 45°$. The maximum width of the second phononic band gap is 12% at $\theta = 25°$. It is worth noting that the two phononic band gaps are separated by the second frequency band of the transverse polarization mode. The width of the partial phononic band gap of the mixed polarization modes increases progressively with an increase in rotation angle, as displayed in Fig. 3(d). The strong tunability of this partial phononic band gap holds great potential for filtering applications.

When compared to existing studies that employ rotation of noncircular cylinders[34,35] or utilize strong external stimuli,[8,39–42] our phononic crystals demonstrate a competitive tuning range for both the position and width of the phononic band gaps. Our results suggest that the reorientation of anisotropic cylinders can serve as a feasible approach for tuning the dispersion relations for acoustic waves propagating in phononic crystals.

B. Hexagonal inclusions: ZnO/epoxy square lattice

Now we consider a two-dimensional, square-lattice phononic crystal consisting of zinc oxide (ZnO) cylinders

embedded in epoxy. ZnO belongs to the hexagonal crystal system and its elastic stiffness tensor has the form

$$c = \begin{bmatrix} c_{11} & c_{12} & c_{13} & 0 & 0 & 0 \\ c_{12} & c_{11} & c_{13} & 0 & 0 & 0 \\ c_{13} & c_{13} & c_{33} & 0 & 0 & 0 \\ 0 & 0 & 0 & c_{44} & 0 & 0 \\ 0 & 0 & 0 & 0 & c_{44} & 0 \\ 0 & 0 & 0 & 0 & 0 & (c_{11}-c_{12})/2 \end{bmatrix}. \quad (17)$$

Acoustic waves propagate in the meridian plane of crystalline ZnO, thus two coordinate transformations with respect to the X and Z axis were applied to the elastic stiffness tensor of the cylinders. Without considering the piezoelectric effect, the slowness surfaces of the three bulk modes at room temperature exhibit a fourfold symmetry shown in Fig. 2(b). After coordinate transformations, the elastic stiffness tensor of ZnO is no longer lower than orthorhombic symmetry, hence the **M** matrix in Eq. (2) cannot be decoupled into two different polarization modes.[28] The three bulk acoustic modes in the phononic crystal are all mixed polarization modes and distinguished as quasi-L, quasi-SH, and quasi-SV modes.

Figure 4(a) shows the calculated dispersion relations for bulk acoustic waves propagating in a ZnO/epoxy phononic crystal with a filling fraction of $f = 0.45$ and a cylinder rotation angle of $\theta = 0$. Note that the irreducible part of the Brillouin zone for the phononic crystal is now rectangular (ΓXMY) due to the fourfold symmetry of the slowness surfaces of ZnO in the meridian plane. It can be seen from Fig. 4(a) that the band diagrams along Γ-X and X-M are different from those along Γ-Y and Y-M, respectively. The arrows point out differences between X and Y at points near the first phononic band gap.

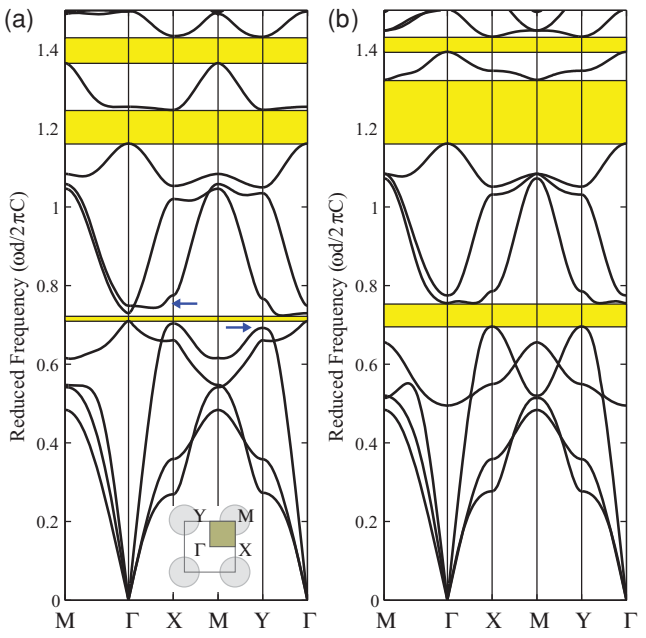

FIG. 4. (Color online) Dispersion relations for bulk modes of a ZnO (meridian-plane)/epoxy square-lattice phononic crystal with a filling fraction of 0.45 and a cylinder rotation angle of (a) 0° and (b) 45°.

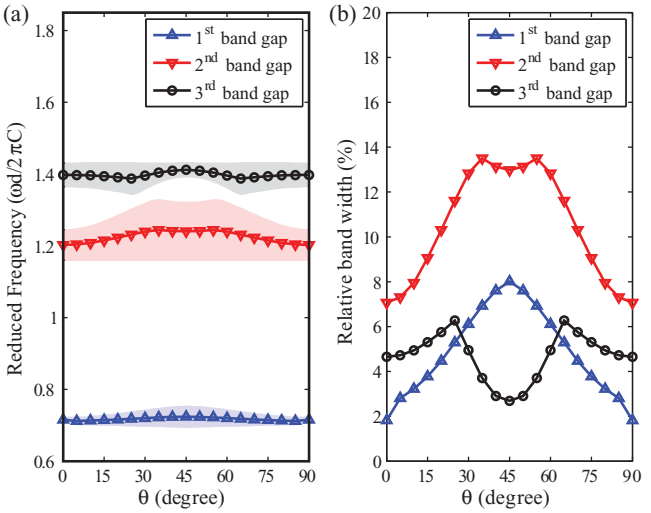

FIG. 5. (Color online) Angular dependence of (a) the midgap frequency and (b) relative bandwidth of phononic band gaps of a ZnO (meridian-plane)/epoxy square-lattice phononic crystal with a filling fraction of 0.45.

In the figure, we observe that three phononic band gaps exist below reduced frequency $\Omega = 1.5$, between the fourth and fifth, seventh and eighth, and eighth and ninth frequency bands, denoted by the yellow colored areas. The midgap frequency (relative bandwidth) of these three band gaps is 0.7155 (1.82%), 1.2025 (7.07%), and 1.3975 (4.65%), respectively. When the ZnO cylinders were rotated 45° in a clockwise direction, the band gaps remained between the same pairs of frequency bands [Fig. 4(b)]. However, the relative bandwidth of the first and second band gaps expanded enormously to 8.01% and 12.98%, respectively, while the third band gap was reduced to 2.69%. Figure 5 displays the geometric dependence of the phononic band gaps in the ZnO/epoxy phononic crystal on the cylinder rotation angle for a range of 0–90°. The solid lines and shaded areas in Fig. 5(a) denote the midgap frequency and the range of the three phononic band gaps, respectively. The relative bandwidths are plotted in Fig. 5(b). At first glance, we notice that all the band-gap parameters are symmetric around 45°; the observed symmetry can be explained by the fact that our calculations account for wave propagation in the entire ΓXMY rectangle of the first Brillouin zone. For example, the dispersion relations along Γ-X at $\theta = 0$ are identical to those along Γ-Y at $\theta = 90°$ due to the fourfold symmetry of the slowness surfaces of ZnO. The width of the first phononic band gap increases monotonically with cylinder rotation angle and reaches a maximum of 8.01% at $\theta = 45°$. The widths of the second and third band gaps also vary with rotation angle, but their maxima appear at $\theta = 35°$ (and $\theta = 55°$ due to the mirror-image symmetry) and $\theta = 25°$ ($\theta = 65°$), respectively. Figure 5 demonstrates that the proposed method can be used to tune the phononic band gaps of a square-lattice phononic crystal consisting of hexagonal cylinders over a considerable range.

C. Trigonal inclusions: Quartz/epoxy square lattice

In this subsection, we investigate a phononic crystal consisting of a two-dimensional square array of quartz cylinders

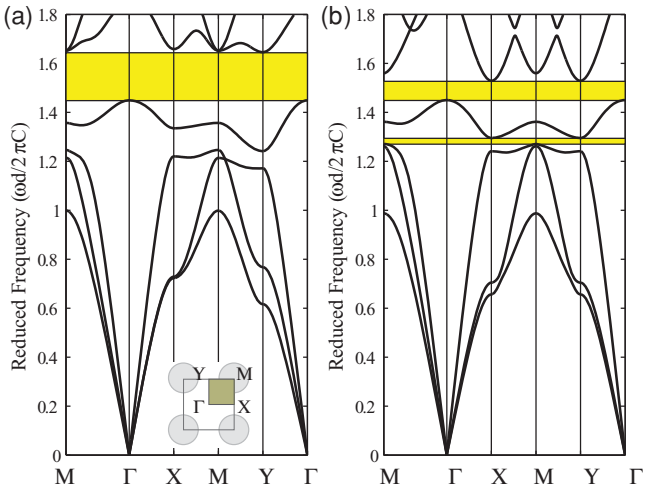

FIG. 6. (Color online) Dispersion relations for bulk modes of a quartz (*XZ* plane)/epoxy square-lattice phononic crystal with a filling fraction of 0.6 and a cylinder rotation angle of (a) 90° and (b) 45°.

embedded in a homogeneous epoxy background. Quartz belongs to the trigonal crystal system, which has six independent elastic stiffness components (see Table I). Bulk acoustic waves propagate in the *XZ* plane [(010) plane] of quartz, thus a coordinate transformation with respect to the crystalline *X* axis was applied to the elastic stiffness tensor of the cylinders. The slowness surfaces of the bulk modes propagating in the *XZ* plane of quartz have a fourfold symmetry, as shown in Fig. 2(c). The dispersion relations of a quartz/epoxy phononic crystal with a filling fraction of 0.6 and a cylinder rotation angle of 90° are shown in Fig. 6(a). In the figure, we observe a wide phononic band gap between the fourth and fifth frequency bands that expands in reduced frequency from 1.448 to 1.644. The midgap frequency and relative bandwidth of the band

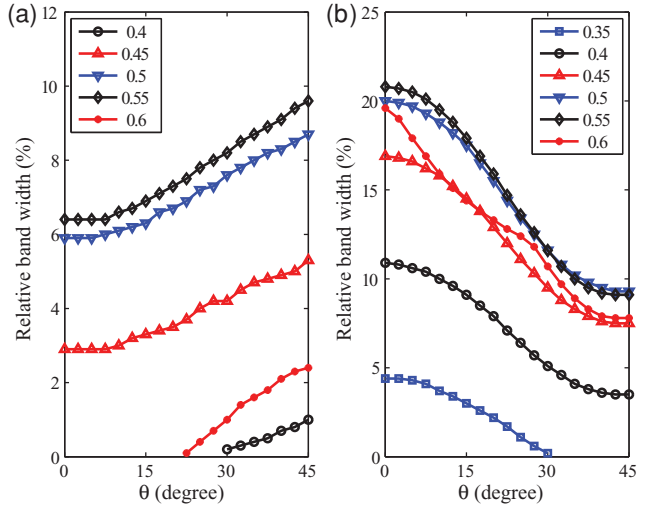

FIG. 7. (Color online) Angular dependence of (a) the midgap frequency and (b) relative bandwidth of phononic band gaps of quartz (*XZ* plane)/epoxy square-lattice phononic crystals with different filling fractions.

gap are 1.546% and 19.6%, respectively. Note that if only the Γ*XM* triangle in the first Brillouin zone is considered, there should be a phononic band gap between the third and fourth frequency bands; however, the overlap of these frequency bands in the *Y*-*M* direction closes this gap. Figure 6(b) shows the dispersion relations when the cylinder rotation angle is 45°. At this cylinder rotation angle the third and fourth frequency bands do not overlap and a phononic band gap opens up, extending from 1.270 to 1.294 with a relative bandwidth of 2.4%. The original phononic band gap remains intact, however, its relative bandwidth of the phononic band gap decreases to 7.8%.

In periodic composite structures, the filling fraction can be another important parameter on band diagram deformation and band-gap modification. Figure 7 shows the relative bandwidth of the first [Fig. 7(a)] and second [Fig. 7(b)] phononic band gaps in the quartz/epoxy phononic crystals as a function of filling fraction and cylinder rotation angle. Only filling fractions ranging from 0.35 to 0.6 (with an increment of 0.05) are shown because no phononic band gap is present in quartz/epoxy phononic crystals outside this range. For any fixed θ, we can see that the width of both phononic band gaps increases with filling fraction, reaching a maximum at $f = 0.55$ (black lines with diamond markers), then decreasing and finally disappearing when $f > 0.6$. In this regard, a quartz/epoxy

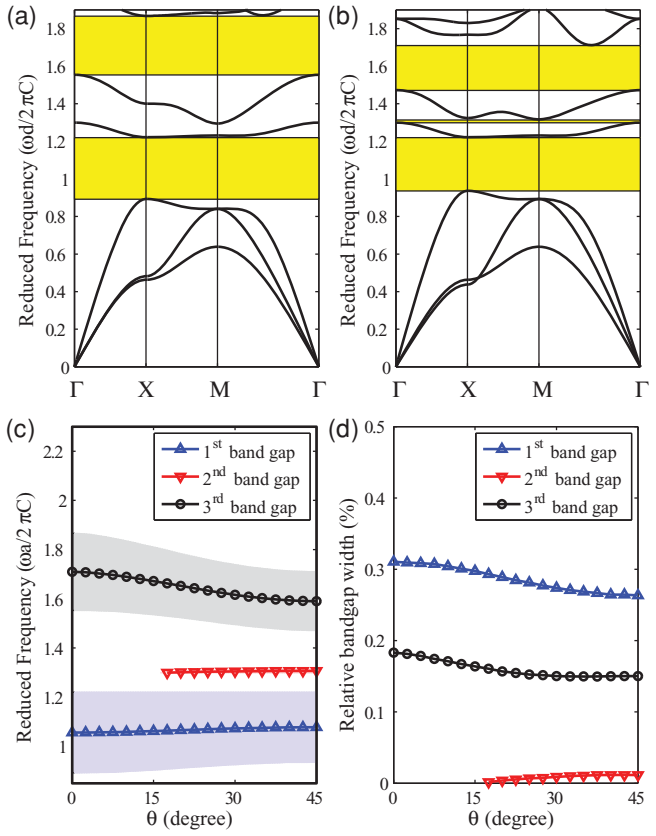

FIG. 8. (Color online) Dispersion relations for bulk modes of a TiO_2 (*XY* plane)/epoxy square-lattice phononic crystal with a filling fraction of 0.5 and a cylinder rotation angle of (a) 0° and (b) 45°; (c) and (d) depict the angular dependence of the midgap frequency and relative bandwidth of the phononic band gaps, respectively.

phononic crystal can be designed with a filling fraction close to 0.55 to obtain the widest possible phononic band gap. For all filling fractions shown in the figure, we observe that the first phononic band-gap width climbs with cylinder rotation angle [Fig. 7(a)], while the second phononic band-gap width declines with cylinder rotation angle [Fig. 7(b)]. In fact, the first band gap of the phononic crystal with $f = 0.4$ and 0.6 does not open until θ increases to 22.5° and 30°, respectively. The second band gap of the phononic crystal with $f = 0.35$ closes when $\theta > 30°$. Therefore by choosing a proper filling fraction and controlling the rotation angle of the quartz cylinders, one can obtain a tunable phononic crystal for filtering or wave-guiding applications.

D. Tetragonal inclusions: TiO_2/epoxy square lattice

Finally we consider a two-dimensional, square-lattice phononic crystal consisting of rutile (TiO_2) cylinders embedded in epoxy. TiO_2 belongs to the tetragonal crystal system that has six independent elastic stiffness components. Bulk acoustic waves propagate in the *XY* plane of crystalline TiO_2 hence no coordinate transformation was necessary. The slowness surfaces of the bulk modes propagating in TiO_2 are shown in Fig. 2(d); they exhibit an eightfold symmetry. The dispersion relations of a TiO_2/epoxy phononic crystal with a filling fraction of 0.5 and cylinder rotation angles of 0° and 45° are shown in Figs. 8(a) and 8(b). Figures 8(c) and 8(d) display the angular dependence of gap position and width, respectively. From these figures, we observe that two wide phononic band gaps exist for all cylinder rotation angles and a very narrow phononic band gap between the fourth and fifth frequency bands opens up at $\theta > 17.5°$. These calculations demonstrate the tunability of phononic crystals composed of cylinders with high anisotropy.

IV. SUMMARY

In this paper, we present a comprehensive study of tunable phononic band gaps in two-dimensional, square-lattice phononic crystals consisting of anisotropic inclusions in an isotropic host. The anisotropic materials considered in this study include cubic, hexagonal, trigonal, and tetragonal crystal systems. Epoxy is employed as the isotropic host material because it allows us to investigate all bulk acoustic wave modes. We have numerically observed that the dispersion relations for bulk acoustic waves propagating in such heterogeneous structures were greatly deformed upon rotation of the anisotropic cylinders. The tunable range of the band-gap width and location demonstrated in this study are competitive with current methods that utilize the rotation of noncircular cylinders and much greater than methods relying on external stimuli. From our theoretical investigations, we suggest that the reorientation of anisotropic cylinders can be a simple and effective way to obtain selective filtering and wave guiding for applications such as acoustic imaging, nondestructive evaluation (NDE), and lab on a chip.[15–19,48–53] Epoxy may constrain the rotational freedom of anisotropic inclusions in a phononic crystal, limit the tunable range of band gap, and thus compromise the performance of the device. Alternatively, anisotropic cylinders can be immersed in gaseous or liquid materials such as air or water to form tunable phononic crystals. Such heterogeneous structures are ideal for audible and underwater applications.

ACKNOWLEDGMENTS

We thank Brian T. Kiraly for helpful discussion and acknowledge the support from the High Performance Computing Group at the Pennsylvania State University. This work was supported by the Air Force Office of Scientific Research (AFOSR), the National Science Foundation, and the Penn State Center for Nanoscale Science (MRSEC).

*junhuang@psu.edu

[1] J. O. Vasseur, B. Djafari-Rouhani, L. Dobrzynski, M. S. Kushwaha, and P. Halevi, J. Phys. Condens. Matter **6**, 8759 (1994).
[2] J. V. Sánchez-Pérez, D. Caballero, R. Mártinez-Sala, C. Rubio, J. Sánchez-Dehesa, F. Meseguer, J. Llinares, and F. Gálvez, Phys. Rev. Lett. **80**, 5325 (1998).
[3] W. Steurer and D. Sutter-Widmer, J. Phys. D **40**, R229 (2007).
[4] R. H. Olsson III and I. El-Kady, Meas. Sci. Technol. **20**, 012002 (2009).
[5] T.-T. Wu, W.-S. Wang, J.-H. Sun, J.-C. Hsu, and Y.-Y. Chen, Appl. Phys. Lett. **94**, 101913 (2009).
[6] Y. Pennec, B. Djafari-Rouhani, J. O. Vasseur, A. Khelif, and P. A. Deymier, Phys. Rev. E **69**, 046608 (2004).
[7] S.-C. S. Lin and T. J. Huang, J. Appl. Phys. **106**, 053529 (2009).
[8] J.-F. Robillard, O. Bou Matar, J. O. Vasseur, P. A. Deymier, M. Stippinger, A.-C. Hladky-Hennion, Y. Pennec, and B. Djafari-Rouhani, Appl. Phys. Lett. **95**, 124104 (2009).
[9] S.-C. S. Lin, T. J. Huang, J.-H. Sun, and T.-T. Wu, Phys. Rev. B **79**, 094302 (2009).
[10] S.-C. S. Lin, B. R. Tittmann, J.-H. Sun, T.-T. Wu, and T. J. Huang, J. Phys. D **42**, 185502 (2009).
[11] T. P. Martin, M. Nicholas, G. J. Orris, L.-W. Cai, D. Torrent, and J. Sanchez-Dehesa, Appl. Phys. Lett. **97**, 113503 (2010).
[12] V. Laude, L. Robert, W. Daniau, A. Khelif, and S. Ballandras, Appl. Phys. Lett. **89**, 083515 (2006).
[13] H. H. Huang and C. T. Sun, New J. Phys. **11**, 013003 (2009).
[14] J.-H. Sun and T.-T. Wu, Phys. Rev. B **76**, 104304 (2007).
[15] Y. Tanaka, T. Yano, and S. I. Tamura, Wave Motion **44**, 501 (2007).
[16] R. H. Olsson III, I. F. El-Kadya, M. F. Su, M. R. Tuck, and J. G. Fleming, Sensor. Actuat. A-Phys. **145-146**, 87 (2008).
[17] X. D. Zhang and Z. Y. Liu, Appl. Phys. Lett. **85**, 341 (2004).
[18] N. Fang, D. Xi, J. Xu, M. Ambati, W. Srituravanich, C. Sun, and X. Zhang, Nat. Mater. **5**, 452 (2006).
[19] M.-H. Lu, C. Zhang, L. Feng, J. Zhao, Y.-F. Chen, Y.-W. Mao, J. Zi, Y.-Y. Zhu, S.-N. Zhu, and N.-B. Ming, Nat. Mater. **6**, 744 (2007).
[20] A. Sukhovich, L. Jing, and J. H. Page, Phys. Rev. B **77**, 014301 (2008).
[21] X. Zhang and Z. Liu, Nat. Mater. **7**, 435 (2008).

[22] J. Pierre, O. Boyko, L. Belliard, J. O. Vasseur, and B. Bonello, Appl. Phys. Lett. **97**, 121919 (2010).
[23] J. Shi, S.-C. S. Lin and T. J. Huang, Appl. Phys. Lett. **92**, 111901 (2008).
[24] S.-C. S. Lin and T. J. Huang, J. Appl. Phys. **106**, 053529 (2009).
[25] Y. Tanaka and S. I. Tamura, Phys. Rev. B **58**, 7958 (1998).
[26] Z.-Z. Yan and Yue-Sheng Wang, Phys. Rev. B **74**, 224303 (2006).
[27] M. I. Hussein, G. M. Hulbert, and R. A. Scott, J. Sound Vibrat. **307**, 865 (2007).
[28] T.-T. Wu, Z.-G. Huang, and S. Lin, Phys. Rev. B **69**, 094301 (2004).
[29] A. A. Maznev and A. G. Every, Appl. Phys. Lett. **95**, 011903 (2009).
[30] J.-C. Hsu and T.-T. Wu, Phys. Rev. B **74**, 144303 (2006).
[31] M. Oudich, M. B. Assouar, and Z. Hou, Appl. Phys. Lett. **97**, 193503 (2010).
[32] Y. El Hassouani, C. Li, Y. Pennec, E. H. El Boudouti, H. Larabi, A. Akjouj, O. Bou Matar, V. Laude, N. Papanikolaou, A. Martinez, and B. Djafari Rouhani, Phys. Rev. B **82**, 155405 (2010).
[33] A. Khelif, P. A. Deymier, B. Djafari-Rouhani, J. O. Vasseur, and L. Dobrzynski, J. Appl. Phys. **94**, 1308 (2003).
[34] W. M. Kuang, Z. L. Hou, and Y. Y. Liu, Phys. Lett. A **332**, 481 (2004).
[35] C. Goffaux and J. P. Vigneron, Phys. Rev. B **64**, 075118 (2001).
[36] Z. L. Hou, X. J. Fu, and Y. Y. Liu, Phys. Lett. A **317**, 127 (2003).
[37] Y. W. Yao, Z. L. Hou, and Y. Y. Liu, Phys. Lett. A **362**, 494 (2007).
[38] K. Bertoldi and M. C. Boyce, Phys. Rev. B **77**, 052105 (2008).
[39] J.-Y. Yeh, Physica B **400**, 137 (2007).
[40] W.-P. Yang and L.-W. Chen, Smart Mater. Struct. **17**, 015011 (2008).
[41] K. L. Jim, C. W. Leung, S. T. Lau, S. H. Choy, and H. L. W. Chan, Appl. Phys. Lett. **94**, 193501 (2009).
[42] Z.-G. Huang and T.-T. Wu, IEEE Trans. Ultrason., Ferroelect., Freq. Contr. **52**, 365 (2005).
[43] A. J. H. McGaughey, M. I. Hussein, E. S. Landry, M. Kaviany, and G. M. Hulbert, Phys. Rev. B **74**, 104304 (2006).
[44] L.-W. Cai, J. Acoust. Soc. Am. **115**, 986 (2004).
[45] D. Torrent and J. Sánchez-Dehesa, Phys. Rev. B **79**, 174104 (2009).
[46] N. Papanikolaou, I. E. Psarobas, and N. Stefanou, Appl. Phys. Lett. **96**, 231917 (2010).
[47] B. A. Auld, *Acoustic Fields and Waves in Solids* (Krieger, Malabar, 1990).
[48] J. Shi, X. Mao, D. Ahmed, A. Colletti, and T. J. Huang, Lab Chip **8**, 221 (2008).
[49] J. Shi, D. Ahmed, X. Mao, S.-C. S. Lin, and T. J. Huang, Lab Chip **9**, 2890 (2009).
[50] D. Ahmed, X. Mao, J. Shi, B. K. Juluri, and T. J. Huang, Lab Chip **9**, 2738 (2009).
[51] D. Ahmed, X. Mao, B. K. Juluri, and T. J. Huang, Microfluid. Nanofluid. **7**, 727 (2009).
[52] X. Mao, S.-C. S. Lin, M. Lapsley, J. Shi, B. K. Juluri, and T. J. Huang, Lab Chip **9**, 2050 (2009).
[53] J. Shi, H. Huang, Z. Stratton, A. Lawit, Y. Huang, and T. J. Huang, Lab Chip **9**, 3354 (2009).